CrossMark

Microstructure Evolution and Microhardness Distribution of Copper Processed Using Multiple Passes of Elliptical Cross-Sectional Spiral Equal-Channel Extrusion

Chengpeng Wang, Daiwang Song, Junkai Fan, and Fuguo Li

The aim of this work is to study the effect of six-pass elliptical cross-sectional spiral equal-channel extrusion (ECSEE) on the microstructure and performance of ultrafine-grained (UFG) copper. Equiaxed grains of average grain size of less than 1 μm are formed into shear bands in the low strain region of ECSEE deformed specimen. More homogeneous and equiaxed microstructure with high misorientation angles is obtained in the high strain. Moreover, the microstructure evolution of ECSEE-induced copper is a dynamic equilibrium process of shear deformation accompanying the interactions of high dislocation density, cellular structure and high-angle grain boundaries. The grain ECSEE refinement mechanism is described as the formation process of dislocations, cells, local grain sub-boundaries rotation and large angle grain restructure. The significantly non-uniform hardness distribution is consistent with the deformation behavior and microstructure refinement in the ECSEE-induced specimen. The homogeneity of microstructure and hardness improves as the ECSEE pass increases.

1. Introduction

Severe plastic deformation (SPD) is a direct method to produce various bulk ultrafine-grained (UFG) materials, including metals, alloys, polymers (Ref 1) and even composite materials with grain sizes smaller than 1000 nm. Different from the traditional plastic methods, such as extrusion, upsetting, drawing and compressing, SPD provides a way to refine coarse grains using intense shear plastic strain in excess of $\sim$ 4-6 and high hydrostatic pressure (Ref 2). Moreover, in contrast to UFG materials produced by the traditional forming methods, those prepared by SPD always have non-equilibrium high-angle grain boundaries (HAGBs), rather than low-angle grain boundaries (LAGBs) (Ref 3). Current SPD techniques include equal-channel angular pressing (ECAP), high-pressure torsion (HPT), multi-directional forging (MDF), etc. (Ref 1, 2). A rod-shaped specimen is pushed through an angular die channel with the equal cross section during the ECAP pressing. The intense plastic shear deformation occurs in the channel intersecting of ECAP die (Ref 4). HPT is quite different from ECAP. A disk specimen is strained by the torsion and high pressure in HPT

(Ref 5). MDF is technically classified as a traditional forging technology by changing the forging axis of 90° pass-by-pass (Ref 6). MDF is usually used for the grain refinement of difficult-to-form metals, such as Mg, Al and Ti alloys. However, additional heating leads to the grain growth. Therefore, how to simplify these processing operations and obtain the unique material properties is a further focus of SPD techniques. Intensive efforts have been directed toward the modification and innovation of SPD methods (Ref 6, 7). According to the forming characteristics, these new methods are mainly categorized as the extension of ECAP or HPT.

The dislocation deformation mechanism (DDM) is one of the most recognized SPD refining mechanisms (Ref 7, 8). High-density dislocations are propelled by the intense shear stress through the movement of different slip systems in DDM model. When the dislocation density of cell walls (CWs) achieves a critical value, the part of dislocations with different misorientations annihilate at the cell boundaries. As a result, excess dislocations remain and form Y-shaped dislocation walls (DWs). Dislocations with Burgers vectors are perpendicular to the boundary. This leads to the increase in misorientation and causes the transformation of granular structures, as the density increases (Ref 2, 7). The dislocations formation of shear zones results in the microstructure of breaking apart. These phenomena were discovered in the study of ECAP, HPT, sandglass extrusion (SE), accumulative roll bonding (ARB) and repetitive corrugation and straightening (RCS). Subsequently, coarse grains gradually evolve into equiaxed cells or/and subgrain structures. The shear-stress dislocation model is also recognized as one of the SPD refinement mechanisms (Ref 3). This grain refinement model is proposed based on the formation of shear bands (SBs) and subgrain rotation. The thin SBs orient along the shear-stress plane. A large portion of dislocation densities and high-angle boundaries form in angle boundaries of initial coarse grains. The movements of shear planes and rotation initiate as the subsequent SPD of materials. The subgrains rotation controls the spatial development of high-angle bound-

Chengpeng Wang and **Daiwang Song**, Institute of Seawater Desalination and Multipurpose Utilization, SOA, Tianjin 300192, People's Republic of China; **Junkai Fan**, School of Mechanical and Power Engineering, Henan Polytechnic University, Jiaozuo 454000, People's Republic of China; and **Fuguo Li**, School of Materials Science and Engineering, Northwestern Polytechnical University, Xi'an 710072, People's Republic of China. Contact e-mail: cpwang2003@foxmail.com.

aries with preferable dispositions during SPD. Moreover, the grain refinement process is due to the mechanical shearing of grains. Equiaxed grains are formed when elongated arrays of grains are subsequently sheared in other directions. Some researchers have found twins as well as dislocations in the simulation of SPD process (Ref 8) and believed that the deformation of nanostructure metals always resulted in the high stacking fault energy (Ref 9). The twins associated with slips are found in the slip deformation process of UFG copper with grain size less than 300 nm. Yamakov and Zhu (Ref 10, 11) further studied the interactions between twinned grain boundaries and dislocation slips in FCC cobalt nanocrystals. They discovered that the twinning deformation had a dual role in the determination of mechanical properties of nanometer grain size materials. Moreover, Gutkin and Fedorov (Ref 12, 13) determined that the deformation of nanoscale metal crystals was due to the grain boundary sliding and torsional deformation modes. The slip dislocations in trigeminal grain boundaries repeatedly break down into climbing grain boundaries along the adjacent edges. This process causes DWs climbing in the grain boundaries and the lattice deforming by the way of rotation transmission in the metal nanoscale-grains.

Elliptical cross-sectional spiral equal-channel extrusion (ECSEE) was proposed as a novel SPD method of various developed SPD techniques (Ref 14). A schematic diagram of ECSEE method is shown in Fig. 1(a). The channel of ECSEE die consists of three segments: Channel L_1, Channel L_2 and Channel L_3, corresponding to the round-ellipse cross-sectional transitional channel, the elliptical cross-sectional torsion transitional channel and the ellipse-round cross-sectional transitional channel, respectively. The ECSEE-processed specimen is subjected to severe plastic deformation as the cross-sectional area remains the constant due to the special structure of die channel. Significant reductions in the grain size are mainly

attributed to high pressure associated with the torsion of ECSEE Channel L_2 (Ref 14-16). The variation of transverse plane of a single-pass ECSEE-processed specimen is described in Fig. 1(b). A round bar specimen is extruded through the cross-sectional transition of the round-ellipse, elliptical cross-sectional torsion and ellipse-round via three die channels (Ref 15). This channel feature of ECSEE die allows the specimen to obtain strain accumulation by repeatedly extruding. Multiple extrusion is essential to refining the microstructure and improving the mechanical properties of SPD deformed materials. Latypov & Seop comparatively analyzed two twist-based SPD processes: ECSEE versus twist extrusion (TE) by means of FEM (Ref 17). The simulation reveals that the stress–strain state imposed in ECSEE twist zones is very similar to those in TE. However, ECSEE requires slightly lower load than that of TE for the extrusion process. The work piece in ECSEE die preserves its geometry better compared to the counterpart in TE die. Moreover, the uniform distributions of maximal plastic strain and equivalent plastic strain are in the ECSEE die.

In previous studies, the simplified slice-plain-strain method and incremental superposition theory were adopted to calculate the effective strain of ECSEE (Ref 18). The ECSEE deformation was divided into two basic deformation modes (Ref 18): round-ellipse/ellipse-round cross-sectional transitional channel deformation and elliptical cross-sectional torsion transitional channel deformation. The research is a mathematical study of plane strain on the deformation characteristics of ECSEE. However, the quantification of effective strain is low available. Current research evaluated the strain value of an arbitrary point in ECSEE-processed specimen (Ref 19). The equation of strain can be expressed as follows.

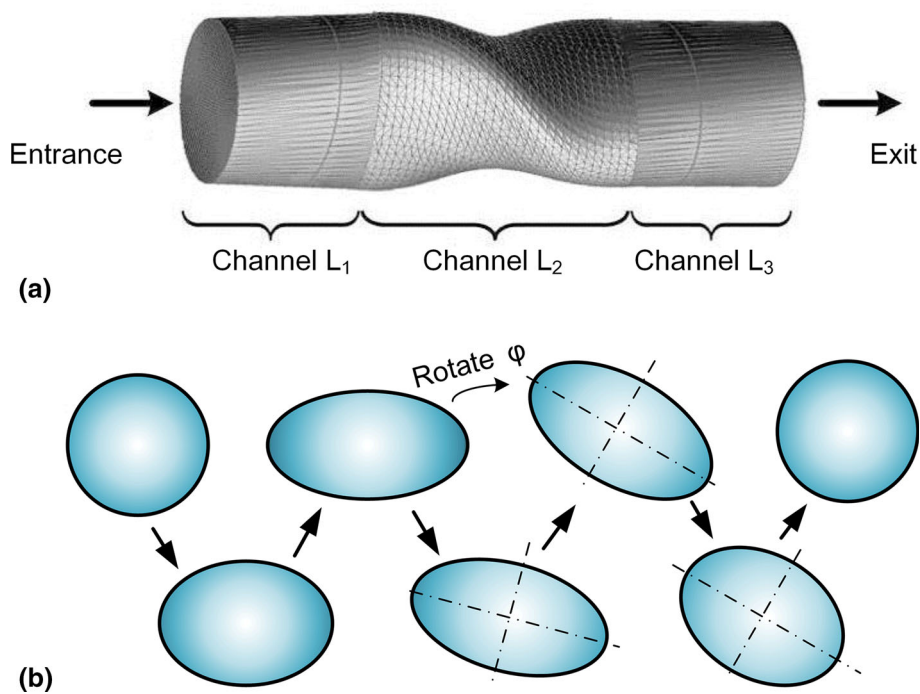$$\varepsilon = \frac{\mu m}{2}\ln\left(1 + \frac{d^2\varphi\sin^2\psi}{4}\right) \tag{Eq 1}$$

Fig. 1 Schematic diagram of (a) the specimen undergoing ECSEE deformation and (b) the variation of transverse plane

where μ is a variable coefficient related to the intrinsic properties of deformation materials such as the hardening index, crystalline structure and alloy phase. ψ is the angle between the line of an arbitrary point and the center point of central axis. φ is the torsional angle. m is the ratio of the major-axis and minor-axis lengths. The variable of m is greater than 1. The letter of d represents the differentiation. The expression is derived for the strain of single-pass ECSSEE. The number of passes, N, should be added in the formula for multiple passes ECSEE deformation. The strain value is strongly concerned with the L , φ and m parameters. Properly speaking, the torsional angle of unit length, and the ratio m are prone to be the decisive parameters for the ECSEE strain accumulation.

The specimen with the dimensions of 10 mm diameter and 30 mm height, and the ECSEE die was a set as following: $D_1 = 10$ mm, $L_1 = 7$ mm, $L_2 = 10$ mm, $L_3 = 7$ mm, $\varphi = 120°$ and $m = 1.55$ (Ref 14). Only Channel L_2 was studied, ignoring of other channels. Hence, the section dimensions are 5 mm × 7 mm. According to Formula (1), the strain is calculated and its values are plotted in Fig. 2. Figure 2(a) shows selected points of calculated strain on the behalf of longitudinal section located in Channel L_2. The area of calculated section is divided into grids. Curves (Fig. 2b) and contours (Fig. 2c) were calculated from the corresponding representative points. The parameter μ is an uncertain value. The value of μ is selected 10 considering the consistency with the numerical simulation in this study. There is further study due to no corresponding theoretical support for the parameter μ. It is still relatively ideal from the perspective regular distribution of Fig. 2(b) and (c). The strain increases with the increase in torsion angle. The gradient distribution state is presented with the distance variation. The strain mainly concentrated on the outer layer of bar specimen, and the internal strain is less. The distribution law conforms to the simulation and real situation, which indicates that the calculated results are ideal and reliable. Li et al. (Ref 20) calculated the average equivalent strain of multi-pass processed specimens after ECAP, ECSEE and torsion deformation. The value of average equivalent strain of ∼ 1 to ∼ 4 in one pass to six passes of ECSEE is slightly lower than the counterpart of ECAP or torsion deformation under the same pass of deformation. The calculated value of using Formula (1) is roughly consistent with the results of finite element simulation under the ideal condition (Ref 14).

The ECSEE method has proven to be an effective method to fabricate bulk copper (Ref 14, 15) and aluminum alloys (Ref 16). Li et al. (Ref 20) compared the deformation modes for ECAP, ECSEE and torsion. The authors classified the deformation modes of bending–torsion, extrusion torsion and pure torsion for microstructure evolution of ECAP, ECSEE and torsion deformation, respectively. In this sense of grain refinement level, ECAP is superior to ECSEE and torsion, while the inhomogeneity is damaged most seriously for torsion, followed by ECSEE and ECAP. The similar refinement process is describe as the formation of SBs, dislocation forest, large angle grain boundaries and subgrains. Wang et al. (Ref 14) numerically and experimentally studied pure copper processed via a single pass using the ECSEE method. The structural parameters of ECSEE die also were optimized based on the grey theory (Ref 21). Existing researches discovered that the ECSEE technology consists of torsional shear, extrusion and upsetting deformation. This combined set of deformation modes is beneficial to the accumulation and conversion of shear deformation during the material SPD processing. The ECSEE-induced specimen undergoes the severe deformation and maintains its original cross section, allowing the specimen to be extruded repeatedly. This deformation feature is very consistent with the characteristic of the aforementioned SPD techniques. Moreover, the ECSEE method overcomes the difficult problem that the forging equipment cannot implement the torsion deformation and reverses the harmful friction into the useful impetus of shear deformation. This advantage of ECSEE is reported in the previous studies (Ref 14-16, 20, 21). Finally, the ECSEE process can be easily installed on any set of standard extrusion equipment by replacing a standard extrusion die with the ECSEE die. The fabrication of UFG materials is of great importance in the academic and industrial points of view. However, there are scarce systematic investigations of the microstructure evolution and grain refinement mechanism of UFG materials fabricated by ECSEE.

In this study, the effects of multi-pass ECSEE on the microstructure evolution and mechanical properties of copper were studied. The ECSEE grain refinement mechanism was described based on observing the formation of deformation bands associated with the dislocation, slip, and GB systems and their interactions. Declaring that the analyses and discussions in this paper are more non-quantitative as a result of the
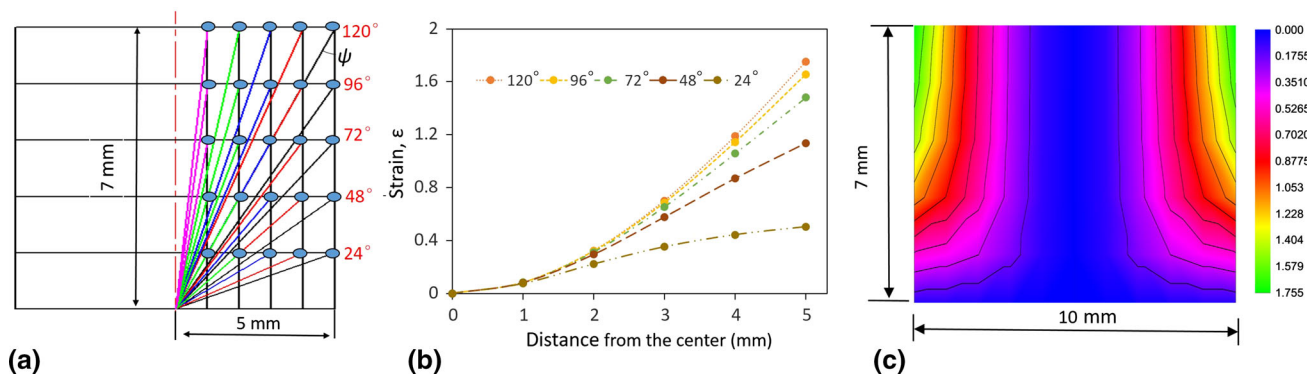

Fig. 2 Strain calculation of (a) selected points, (b) curve of strain vs. distance and (c) strain contours

complexity of forming and experiment condition in current stage.

2. Experimental Procedure

The commercial copper specimens were preconditioned by annealing at 400°C for 2 h and then furnace cooled to obtain a grain size of 100 μm. The average microhardness for the starting (initial) pure copper is ~ 40 HV. The received specimens were machined to a diameter of 10 mm and a length of 30 mm for subsequent processing. To obtain the same equivalent plastic strain, the cavity parameters of ECSEE die were set based on the work of previous studies (Ref 14). The ECSEE experiments were conducted over six passes at room temperature with the extrusion speed of 1 mm/s using the lard lubrication. Multi-pass ECSEE-processed specimens were symmetrically wire-cut into horizontal and vertical segments. The segments were subjected to coarse grinding and fine grinding with a waterproof abrasive followed by the mechanical polishing with diamond powder. For OM observation, the specimens were etched with a solution containing $FeCl_3$, HCl and H_2O (at a ratio of 1:3:20) for 10 s.

The thin foils for TEM observations were cut from the longitudinal section of specimens, mechanically ground to approximately 40 μm, and finally thinned using a precision ion polishing system (Model 691 PIPS, GATAN Inc.). The microstructure observations were performed on a Tecnai G2 S-Twin F30 high-resolution TEM (HRTEM, 300 kV, FEI Company). The measurements of cell sizes were made directly from TEM observations, and the reported values are averaged from approximately ~ 100 cells selected randomly from each specimen. The cell size was measured along two axes of parallel and perpendicular. The grain diameter was estimated by measuring and averaging the length and width of the strongly diffracting grains using Image-Pro Plus software (Ref 22). Then, the grain size distributions were plotted from the data of grain diameter.

The dislocation density ρ in the grains of the specimens was evaluated by Ham's intersection method (Ref 23). The first procedure is a mesh drawn on a TEM image of a grain satisfying the diffraction condition, and then the number of intersections n between the mesh and dislocations is counted. The dislocation density was evaluated using Eq 2 (Ref 23).

$$\rho = 2n/Lt \tag{Eq 2}$$

Here, t is the thickness of the specimens and L is the total length of the measured mesh. To reduce the error of the invisible dislocations, TEM specimens were tilted (0-2°) in order to observe the highest number of dislocations within a grain.

The microstructure was studied along the longitudinal section for different deformation conditions using a scanning electron microscope (JEOL JSM-7001 F Field Emission) equipped with the Oxford Instruments HKL Channel 5 software package for EBSD measurement. Different step sizes of 0.05 μm were used. Misorientations less than 3° were not considered during post-processing. ECSEE specimens were examined by EBSD in the marginal area of longitudinal direction.

Vickers microhardness (HV) tests were employed using 100 g loads and the dwell time of 15 s with a HXP-1000TM microhardness tester. The HV was investigated at seven selected points along the centerline of the longitudinal sections. All selected points were measured five times with the average value reported.

3. Results and Discussion

3.1 Optical Metallographic Observations

OM micrographs of pure copper after six passes of ECSEE deformation are shown in Fig. 3. The obvious shear zones in the circumferential areas are shown in Fig. 3(b) and (d). The distributions of flow lines on the cross-sectional and longitu-
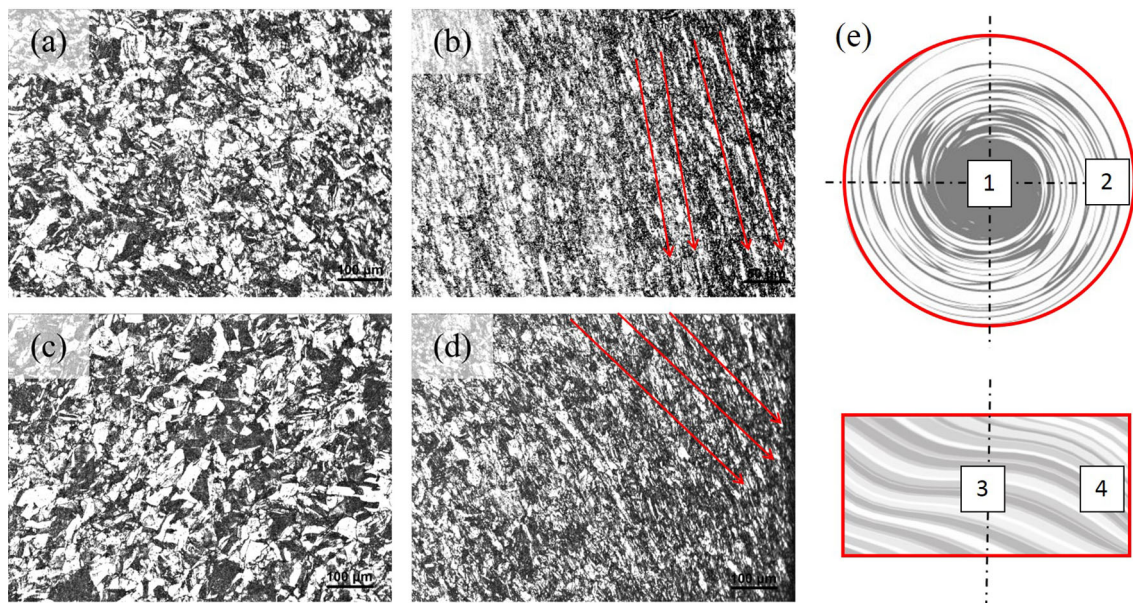

Fig. 3 OM micrographs of multi-pass ECSEE-processed copper: (a) the center of cross section (label 1), (b) the circumferential edge of cross section (label 2), (c) the center of longitudinal section (label 3) and (d) the edge of longitudinal section (label 4)

dinal section are shown in Fig. 3(e). The observed positions are separately labeled with numbers. The flow lines on the cross section present a gradient distribution state of swirling. The flow state is obvious in the peripheral part (label 2), while the counterpart in the central part (label 1) is little due to small deformation. Hence, the change in internal flow is unobvious. The distribution of flow lines presents the morphology of plates or/and strips in the longitudinal section. The streamlines are along the tangential direction of shear stress in edge part (label 4). The streamlines are paralleled and have less tilt along the tangential direction in internal part (label 3). Grains in the circumferential areas are significantly refined with shear zones, which are compared to their counterparts in the center position, where no significant shear zones are found (see Fig. 3a and c). The vortex appearance of metal flow lines on the cross section of specimen is similar to the feature of torsional microstructure. The direction of flow lines is always along the shear direction. However, the flow lines on the longitudinal section of specimen are not the skew lines like the torsion deformation feature (see Fig. 3b and d). The interpretation may be ascribing the spiral line of the space forming in the ECSEE-induced specimen. The offsetting effect on the central area increases in the multiple passes of ECSEE, and the flow lines are more parallel. Due to more severe shear deformation significantly, the grains in the circumferential areas are greatly extended and even broken into a fragmented substructure. The torsional shear deformation, especial in Channel L_2 of the ECSEE die, plays a significant role in the refinement of ECSEE-processed materials. Simple shear deformation consists of a series of parallel sliding layers formed by shear slippage. The deformation mode of the ECSEE is an inhomogeneous one, similar to pure torsion. Both the stress and strain are transmitted from the bar specimen surface into the interior via the torsional loading. Previous research has shown that the value of the torsion strain changes incompletely linearly from zero at the center of the bar specimen to a maximum value at its surface. The "oval" shape of strain distribution is matched with the elliptical cross-sectional shape of the die channel (Ref 14, 15). The effective strain in left–right area of cross section is higher than that in the above-under area. The distribution pattern of effective strain is especially possibly due to the severe shear deformation in region of ellipse major-axis, while the area near ellipse minor-axis is subjected to less severe shear deformation. The effective strain in the ellipse major-axis area of cross section is higher than that in the minor-axis area and central area. However, the severe shear deformation in the external region of ECSEE-induced specimen is more than the counterpart in the internal region. Numerous investigations have shown that a homogeneous of microstructure refinement could improve as the torsion rotation increases (Ref

24). Accompanying the ECSEE deformation, these fragmented grains are distributed along the shear direction and exhibit a strong filamentary structure in the macro-level. The granulated isometric grains gather along the long strips of the sheared microstructure. The SBs or laminate structure progressively develops along the flow direction. The microstructure characteristic is quite similar to that formed during cold-rolling deformation (Ref 25) and multi-pass ARB deformation (Ref 26).

3.2 EBSD Observations

EBSD has become a standard material measurement technique to effectively determine the information of morphological parameters, such as grain size and shape distributions. Figure 4 shows the orientation imaging microscopy (OIM), misorientation distribution and selected EBSD regions of copper after being selectively processed by one, three and six passes of ECSEE. In this study, the textures were represented in the TD-ND-ED reference system. The normal direction of ND is perpendicular to the extrusion direction. The extruded specimen was distorted on the ED-TD plane in Channel L_2 of ECSEE die. The unit triangle shows the colors corresponding to different grain orientations. The HAGBs with misorientation angle greater than 15° are shown as black lines and LAGBs with misorientations between 3° and 15° are shown as white lines. Figure 4(a) presents an initial microstructure of copper prior to ECSEE. The twin boundaries are the type of dominant grain boundary. The average grain size statistics by EBSD was larger than 40 μm with well-defined grain boundaries and twins in interior of grains. The elongated grains or deformation bands and a small number of well-developed subgrains exhibit in the microstructure of one pass of ECSEE-induced specimen as shown in Fig. 4(b). The deformation bands are generally associated with the shear strain process (Ref 27). In the low strain, an operative slip system originates in the polycrystalline material. More numbers of slip systems may operate as the deformation increases. The different sets of slip systems lead to different lattice rotations to coordinate the strain imposed into the materials. The more heterogeneous microstructure forms with plenty of grains, whose average grain size is several micrometers or even nanometers after three and six passes in Fig. 4(c) and (d). However, the mixture coarser subgrains present in some regions in three and six passes of ECSEE-induced specimens. The high deformation led to the transformation of cell boundaries into subgrains, but a significant fraction of LAGBs persists around coarser grains. In the SPD process, the grain refinement of the bulk material usually reaches a level of equiaxed ultrafine (≤ 1 μm) or nanoscale

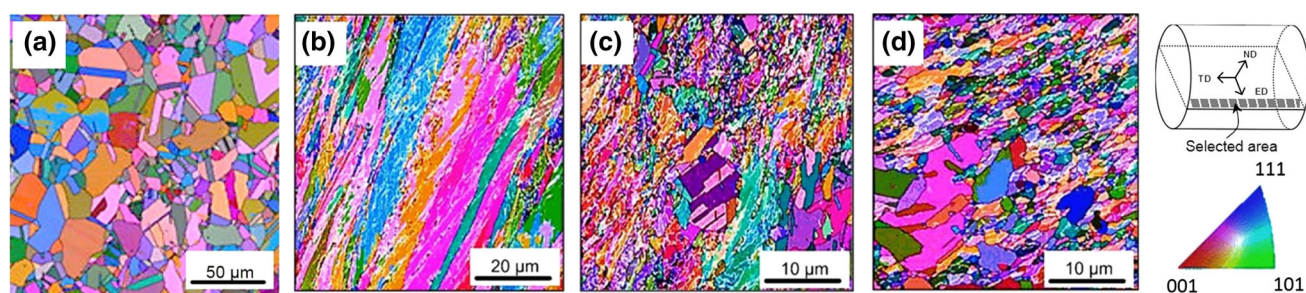**Fig. 4** OIM and misorientation distribution, including subgrain boundaries (SGBs) (3° ≤ θ < 15°, white lines) and grain boundaries (≥ 15°, black lines) of copper (a) initial, and processed by ECSEE after (b) one pass, (c) three passes and (d) six passes

(≤ 100 nm). Elongated, ribbon-like dislocation cells (DCs) or subgrain structures form in the smaller equivalent strain in SPD at low homologous temperatures and evolve into highly refined equiaxed structures in larger strain. These results are similar to those from other studies on ECAP processed copper (Ref 27, 28).

Figure 5 shows the histograms of misorientation angle (Fig. 5a, b and c) and statistical variation of grain size (Fig. 5d, e and f) taken from a scan on edge regions of specimens' section. The statistical data and selected EBSD regions are from Fig. 4. For one pass, the fraction of large angle boundaries increases significantly and being a small percentage. It is an indication that the formation of cells and subgrains are in existing grains. For three passes, the subgrain misorientations increase, and a balanced distribution is in LAGBs and HAGBs. For six passes, the LAGBs are in a minority, and the orientation distribution tends to be high. In the plastic deformation of material, the dislocations need to accommodate the misorientation of neighboring cellblocks (CDs). The DC boundaries are also known as the incidental boundaries due to the statistical mutual tapping generation of gliding dislocations (Ref 29). In the SPD process, the misorientation increase leads to the formation of new HAGBs, and the percentage of subgrains increases in the high strain. Grain fragmentation usually depends on the grain orientation of special orientation symmetry (Ref 30). As demonstrated in Fig. 5(d)-(f), the grain size decreases with the increase in deformation passes. More and more grains are less than 1 μm. The average grain sizes are ∼ 0.7 μm, ∼ 0.5 μm and ∼ 0.4 μm for one, three and six passes, respectively. The statistical variation of grain size shows an evidence for the ECSEE grain refinement as shown in Fig. 4. The general appearance of these distributions is consistent with those earlier reported (Ref 27).

In the above analysis, the ECSEE deformation leads to the grains shearing and is accompanied by an increase in the fraction of substructures and misorientation. The misorientation increase is within the deformation bands and in the formation of new HAGBs. The grain boundary distribution changes from a high portion of LAGBs after the one pass of ECSEE to a high portion of HAGBs after six passes. The ECSEE strain causes the polygonization and the transformation of substructure into a granular-type microstructure accompanied by a dramatic grain size reduction.

3.3 TEM Observations

Figure 6 shows the TEM observations of copper after the multi-pass ECSEE process. For the low strains after one pass of ECSEE, the microstructure mainly consists of dislocations, SBs and DCs structure (see Fig. 6a). The microstructure after one pass of ECSEE consists of strongly elongated subgrains with the mean SBs or lamellar boundaries (LBs) spacing of ∼ 500 nm. The boundaries of DCs are seen inside LBs or/ and SBs. The dislocation tangles are clearly observed in CWs. SBs have a tendency to line up parallel with the shear direction. The structures of DCs or/and CWs show the increasing dislocation motion caused by the dislocations escaping from the tangles due to the cross-slips, which are responsible for the plastic deformation in the low strain (Ref 31). In the intense plastic deformation, the generation of DCs extends from the margin to the interior of original grains. The deformed SBs are separated by the geometrically necessary boundaries (GNBs). Except for the GNBs, the other boundaries are incidental dislocation boundaries (IDBs) (Ref 32), which usually form within a grain by the statistical trapping of dislocations. The GNBs accumulate dislocations at a higher rate than IDBs. Hence, the density of grain boundary dislocation is greater than the counterpart of intragranular dislocation.

As the strain increases further (two passes, Fig. 6b), the width of SBs decreases significantly, whereas the quantity of DCs and CWs increases. The quantity of DCs and CWs increases with the increase in shear strain. By contrast,
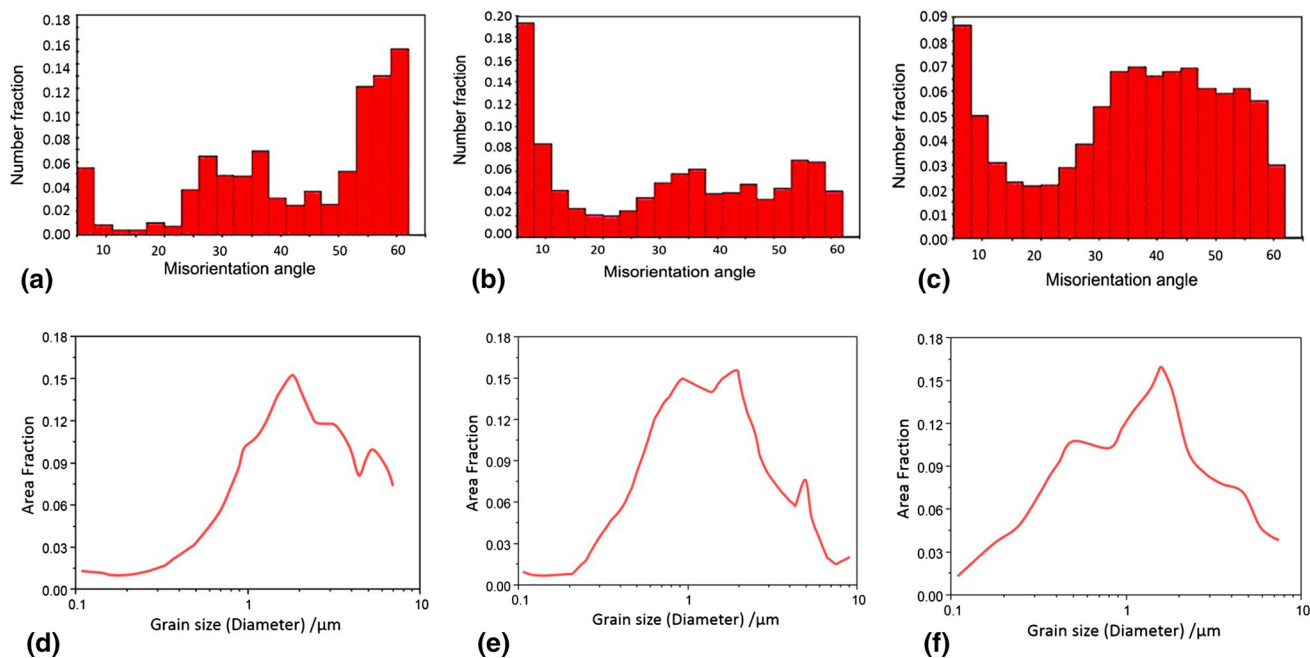

Fig. 5 The histogram of misorientation angle and statistical variation of grain size of ECSEE-produced specimens: (a) (d) one pass, (b) (e) three passes and (c) (f) six passes
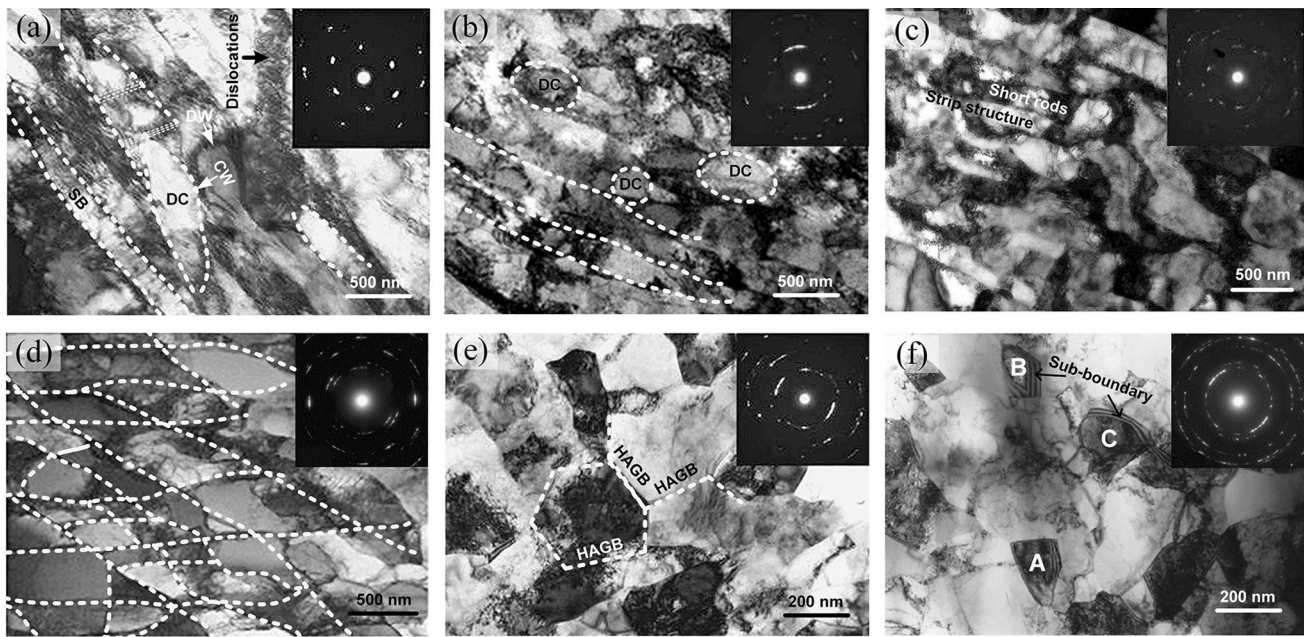
Fig. 6 TEM images of pure copper processed by multi-pass ECSEE: (a) one pass, (b) two passes, (c) three passes, (a) four passes, (e) five passes and (f) six passes

approximately 50% of area belongs to the structure of DCs and CWs in two passes of specimen, and a more uniform microstructure is attained in two passes due to the decrease width of LBs or/and SBs. A similar observation was found in the microstructure induced by the process of rolling or RCS (Ref 33).

For three passes of ECSEE deformation (shown in Fig. 6c), the obvious DW boundaries appear in SBs, and the entire microstructure distribution appears similar to a brick wall. The area fraction of short rods and strips structure is about 70% after three passes. The microstructure is more homogeneous than that of two passes of specimen. The similar DCs in the CDs are usually interconnected to form a cellular network in the microstructure produced by rolling or RCS (Ref 34). The long strips structure ruptures into tiny short rods. This interpretation is ascribed to the different slip system number, which could coordinate the deformation within the grain area. Thus, the elongated grains can be separated into small grain fragments through the transition zone of dense DWs or GNBs fragmentation (Ref 35). As described, an additional slip system may be triggered in the cells as the strain increases. More and more DCs act like CDs, and the subgrain structures become separated (Ref 36). With the further deformation, many subgrains may further divide into smaller ones, and the misorientation between subgrains may increase to form LAGBs and HAGBs (see Fig. 4).

After four passes of ECSEE (in Fig. 6d), the reverse inclination deformation occurs to the short rod-like grains. The microstructure of no much-elongated grains is found, which means the achievement of more equiaxed microstructure. Unlike the rolling-induced microstructure, the DCs are not well networked. Parallelogram or diamond-shaped subgrains come into being. Interestingly, although the segment of LAGBs is in the non-equilibrium configuration, another segment is in an equilibrium configuration without any extrinsic dislocations. It is not clear whether the grain boundaries orienting along a low index plane tend toward an equilibrium state. Such boundaries are unstable and may reconfigure to form equilibrium boundaries.

The equiaxed grains appear, and no obvious dislocations exist in the vast majority of grains in Fig. 6(e). The subgrains mainly present the equiaxed appearance. However, the exhibited microstructural inhomogeneity is in the feature of subgrains lying in close vicinity. Some areas of particular grains are found completely dislocation-free as opposed to neighboring regions, which are heavily deformed. Grains with heavy dislocation densities can be fragmented into finer grains affected by strain. However, there is still a high dislocation density within some individual grains. The dislocation tangles can be clearly observed in the grain boundary area through the boundary slips. In addition, the feature of straight grain boundaries and LAGBs is obvious in the initial grains with low dislocation density. Therefore, the large angle grain orientations eventually form through the similar polygons and are annexed by the interacting subgrains in the grains with a high dislocation density.

A micrograph after six passes of ECSEE deformation is shown in Fig. 6(f), no obvious dislocations exist in the vast majority of interior grain microstructure. Most of the grain interfaces are thin, clear and flat, and the majority of grain size is 200-300 nm. In Fig. 6(f), the equiaxed degree of grains A and B is apparently less significant than that of grain C. The Moiré fringes around subgrain boundaries are caused by low-angle misorientations of neighboring grains along the TEM electron beam direction. The presence of non-equilibrium grain boundaries (Ref 3) was previously documented in materials processed by HPT (Ref 5, 37) and ECAP (Ref 23, 27).

Fine equiaxed grains with HAGBs were observed in copper after large plastic strains at room temperature using the combination of torsion and compression (Ref 37). Moreover, similar to the microbands observed in the rolling-induced microstructure of copper (Ref 25, 33, 34), two-stage generated microbands compose the chessboard microstructure. In the multi-pass ECSEE process, the slip systems could change when

the strain path changes from one pass of ECSEE to the next. Consequently, the dislocations not only interact with other dislocations in the current active slip systems but also interact with inactive dislocations generated from the previous ECSEE pass. With the ECSEE strain increases, the isolated DCs may become the isolated subgrains. The misorientation across the SGBs increases with the further ECSEE strain and eventually becomes large enough to transform the SGBs into LAGBs or HAGBs.

Diffraction experiments of ECSEE-induced specimens with different passes are performed over the bright phase region. The diffraction phase zones are shown on the right top of Fig. 6. In the low strain, the highlighting short dispersion curves of diffraction spots illustrate that the grain boundary mainly consists of small interfacial angles. As the forming passes increase, the material distortion increases, and the diffraction spot elongates. The diffraction spots gradually evolve into the continuous loops, showing that as the deformation increases, the grains are effectively refined with the HAGBs.

The histograms of the grain size distribution that ranges from 200 to 890 nm are demonstrated in Fig. 7. The range of grain size expands the small trend with the increase in passes. The grain sizes measured by TEM are often larger than those measured by EBSD.

Figure 8 shows the variation of average dislocation density and average cell size of ECSEE-processed specimens. The cell size measured indicates a dramatic decrease in the course of one pass to two passes, and the gradual variation tendency presents after the subsequent passes. In contrast, the dislocation density increases until the three passes of ECSEE, at which a maximum value of $\sim 1.7 \times 10^{14}$ m^{-2} reaches. The density value follows by a decrease to a value of $\sim 1.1 \times 10^{14}$ m^{-2} after six passes.

In the SPD deformation, the high-density dislocations are impelled by the intense strain of deformed materials by the movement of different slip systems. When the dislocation density in the cell walls reaches a certain critical value, part of dislocations can annihilate at the cell boundaries. As a result, the thickness of dislocation wall becomes thin and the cell size decreases. As the dislocation cell size tends to a saturated value with the continued plastic strain, a saturated grain size equivalent to the minimum cell size is expected with the strain increasing. The coarse grains gradually evolve into equiaxed cells and subgrain structures. The shear-stress dislocation model (Ref 8) above of the SPD refinement mechanism can be used to explain on the increase in misorientation and cause
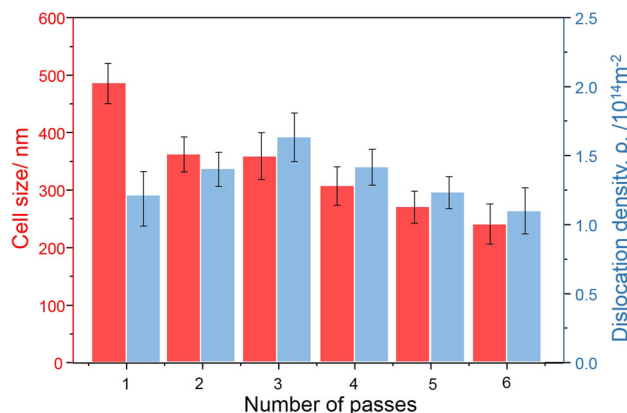

Fig. 8 Cell size and dislocation density measured plotted as a function of the number of ECSEE passes
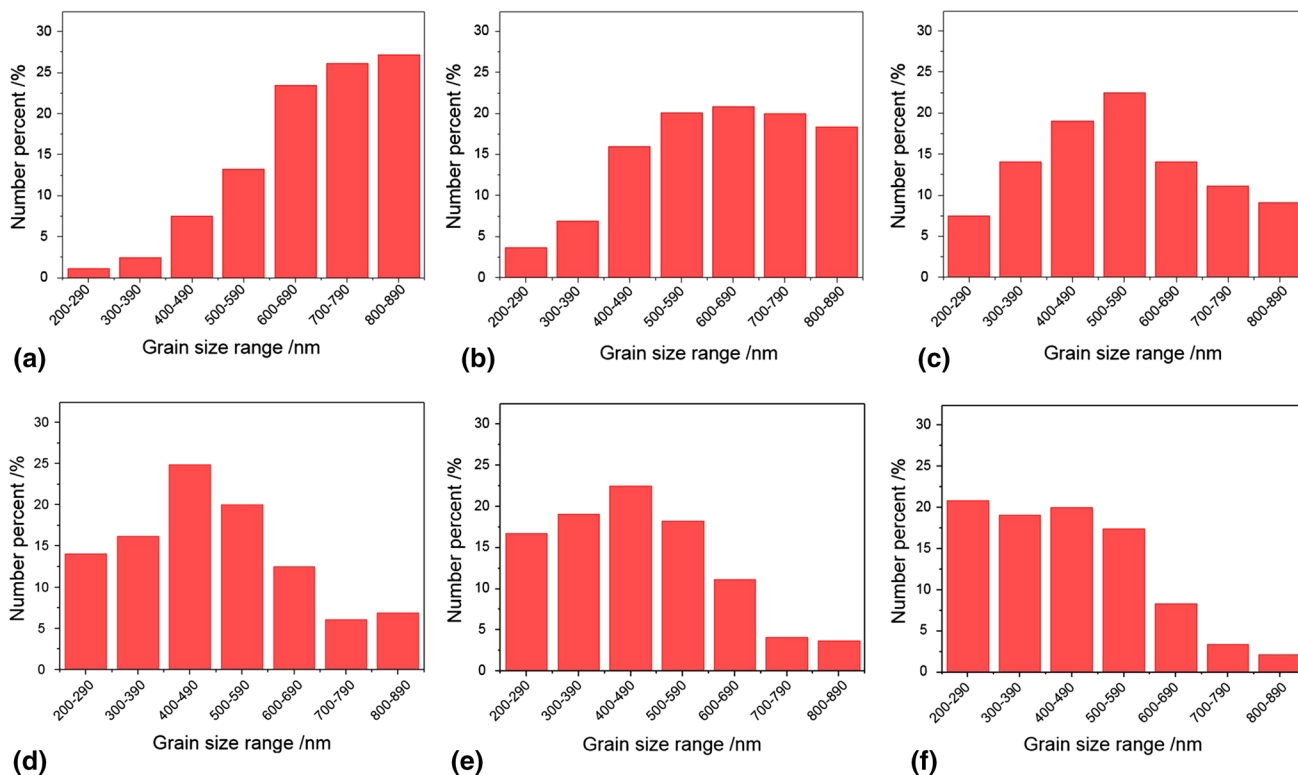

Fig. 7 Grain size distributions of copper after ECSEE passes: (a) one pass, (b) two passes, (c) three passes, (a) four passes, (e) five passes and (f) six passes

the transformation to the granular structure when the density increases. The cell sharp becomes more equiaxed gradually with the increase in ECSEE pass (see Fig. 6).

Many models have described the deformation of polycrystalline materials. Taylor's model is the most appropriate for the formation of equiaxed grains (Ref 31). Three kinds of grain refinement mechanisms (Ref 7, 8): strain-induced grain refinement, thermal mechanical deformation refinement and particle refinement are popular in current SPD research. It is generally accepted that the grain refinement is caused by dislocation gliding, accumulation, interaction, tangling and spatial rearrangement in SPD-induced materials. Li et al. (Ref 20) comparatively investigated the different SPD modes of ECAP, ECSEE and torsion, and classified these as the combined bending–torsion, combined tension–torsion and pure shear. The torsion shear is typical one for ECSEE and TD, while tensile breaking off for ECAP. Under the high passes deformation, ECSEE showed double twist broken configuration, TD has a single twist broken configuration, and ECAP retains the straight grain refinement pattern. The authors consider this classified method of forming mode is less rigorous. Normal strain and shear strain are the basis of plastic deformation mechanics. Simple shear is of significance in the refinement of SPD-induced material (Ref 35). Simple shear leads a short stage of continuous evolution in the localization, and intensive strain is mainly located in the SBs. The cross-loading results in the spatial networks of HAGBs. Similar to the combination of torsion and compression, ECSEE provides a nearly uniform simple shear with monotonic loading along fixed planes. The SPD refinement mechanism is so complicated that no unified theory system has emerged. Further investigations are required to describe the SPD refinement mechanism.

3.4 Grain Refinement Mechanism of ECSEE

As confirmed by the OM, TEM micrographs and SAD patterns as well as the EBSD analysis, the increase in dislocation density and its accumulation in SBs and cell structure (Fig. 8) at low levels of strain in low pass of ECSEE. The increase in misorientations (Fig. 4a) by strain-induced transition of LAGBs to HAGBs with further ECSEE strain. As can be seen in Fig. 4 and 6, a large fraction of LAGBs is formed after the initial deformation. As the pass increases, the misoriented subgrains are more refined, the fraction of HAGBs considerably increases. The spacing of dislocation or/and grain boundaries decreases, and their misorientations increase by accumulating strain. A homogeneous microstructure of

equiaxed grains is finally achieved at high levels of ECSEE strain. It is concluded that the microstructure development taking place during ECSEE is similar to the common mechanism of strain-induced grain refinement in copper processed by other SPD approaches (e.g., cold-rolling (Ref 25), ECAP (Ref 23, 27, 29) and HPT (Ref 37)). Grain refinement induced by plastic strain in metals is a well-known phenomenon (Ref 33). Saturated grain sizes can be reached with increasing strain when the recovery grain coarsening and the strain-induced grain refinement are balanced.

3.5 Microhardness Examination

Hardness partly reflects the material's resistance to plastic deformation. The content of grain refining and dislocation is attributed to the hardness of SPD-induced materials. Figure 9(a) shows the microhardness distribution along the radial direction on the cross section for a multi-pass ECSEE deformed specimen. The characteristics of gradient distribution are obvious as the distance from the center point increases. The hardness value is low in the center of specimens, whereas it is greater near the surface area of specimen. Figure 9(b) shows the hardness differences from two to six passes and one ECSEE pass. On the areas closer to the specimen surface, the differences in the hardness are smaller. This indicates that the strengthen saturation is easy to achieve on the surface of the deformed specimen. As the deformation increases, the reinforcement saturation gradually transits from the surface to the interior of the bar specimen. As shown in Fig. 9(b), the distance 1 mm from the center, the hardness increases with the number of passes. The increase occurs more rapidly at the inner position, in contrast to that for the bar-specimen periphery. To summarize, the hardness first reaches saturation at the bar-specimen surface due to the characteristics of non-uniform ECSEE deformation. As shown in Fig. 1, the ECSEE deformation mode is similar to the torsional deformation. Both modes have an inhomogeneous strain distribution. This manner leads to the inhomogeneous hardness distribution observed over the cross section of ECSEE-induced specimen. The deformation uniformity and the reinforcement effect can effectively improve as the deformation passes increase (Fig. 9b). Mishra et al. (Ref 36) summarized the hardness as a function of number of ECAP passes (data from different sources). The hardness value of ~ 114 to ~ 143 Hv corresponds to the specimen processed by 3 to 12 passes of ECAP. Lugo et al. (Ref 37) measured the Vickers microhardness of the samples processed by eight passes of ECAP and five turns of
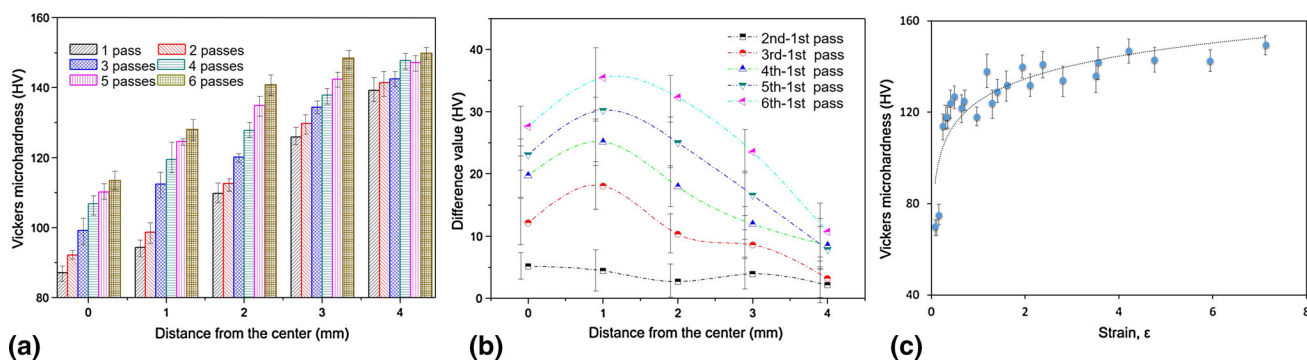

Fig. 9 (a) Hardnesses plotted against the distance, (b) hardness differences plotted against the distance and (c) hardnesses plotted against the strain

HPT to be ~ 152 and ~ 150 Hv. The hardness saturation of ECSEE is consistent with the above research data. Figure 9(c) shows the statistical graph of microhardness versus strain resulting of specimens in the distance from 1, 2, 3 and 4 mm. The microhardness values as a function of strain give a unique relation. The hardness increases up to a strain of ~ 4, and thereafter, there is only a minor increase in hardness and ultimately the hardness saturates at ~ 145 Hv. Furthermore, it should be noted that we have found similar results also for other SPD-induced materials.

This phenomenon can be primarily attributed to a decreasing grain size accompanied with an increasing dislocation density. Furthermore, for the single ECSEE pass, the increase in microhardness at the relatively low strain seems to be attributed to the strain hardening from dislocation and/or SGBs formation rather than grain refinement (Ref 14, 15). However, the grain boundary strengthening becomes more and more prominent. For cold-deformed metals (Ref 38), the strength–structure relationship can be typically described by the dislocation strengthening and the boundary strengthening. The strengthening of grain boundary is related to the parameter of the average grain size of deformed material (Ref 39), which is predicted from the average grain boundary misorientation angle (Ref 40). It appears that the critical angle plays an important role in estimating the strengthening mechanism. As shown in Fig. 9, the strengthening becomes weaker from the saturation of dislocations and the grain refinement limit.

4. Conclusions

The deformation characteristics, microstructure evolution and mechanical properties of pure copper subjected to the multi-pass ECSEE process were studied using OM, EBSD, TEM and microhardness measurements. The following conclusions were determined as follows.

1. The grain refining process of the ECSEE technique is a severe non-uniform deformation process. The elongated grains with an average grain size of less than 1 μm are obtained in the low strain, whereas a more homogeneous and equiaxed microstructure with a higher misorientation angle is observed in the high strain.
2. The hardening/strengthening on the specimen surface first reaches saturation due to the non-uniform characteristics of the ECSEE deformation mode. The uniformity is effectively improved as the number of ECSEE passes increases.
3. The microstructure evolution of the ECSEE deformation is a dynamic equilibrium process induced by the shear deformation associated with high dislocation density, cellular structure, LAGBs and restructuring large angle grains.

References

1. X. Zhang, X. Wu, H. Haryono, and K. Xia, Natural Polymer Biocomposites Produced from Processing Raw Wood Flour by Severe Shear Deformation, *Carbohydr. Polym.*, 2014, **113**(113), p 46–52
2. R.Z. Valiev and A.K. Mukherjee, Nanostructures and Unique Properties in Intermetallics, Subjected to Severe Plastic Deformation, *Scr. Mater.*, 2001, **44**(8–9), p 1747–1750
3. R.Z. Valiev, Y.V. Ivanisenko, E.F. Rauch, and B. Baudelet, Structure and Deformaton Behaviour of Armco Iron Subjected to Severe Plastic Deformation, *Acta Mater.*, 1996, **44**(12), p 4705–4712
4. S.E. Mousavi, M. Meratian, and A. Rezaeian, Investigation of Mechanical Properties and Fracture Surfaces of Dual-Phase 60–40 Brass Alloy Processed by Warm Equal-Channel Angular Pressing, *J. Mater. Sci.*, 2017, **52**(13), p 8041–8051
5. J.M. Rosalie, J. Guo, R. Pippan, and Z. Zhang, On Nanostructured Molybdenum–Copper Composites Produced by High-Pressure Torsion, *J. Mater. Sci.*, 2017, **52**(16), p 9872–9883
6. R. Łyszkowski, T. Czujko, and R.A. Varin, Multi-Axial Forging of Fe3Al-Base Intermetallic Alloy and Its Mechanical Properties, *J. Mater. Sci.*, 2017, **52**(5), p 2902–2914
7. C.P. Wang, F.G. Li, W. Lei, and H.J. Qiao, Review on Modified and Novel Techniques of Severe Plastic Deformation, *Sci. China Technol. Sci.*, 2012, **55**(9), p 2377–2390
8. C.P. Wang, F.G. Li, B. Chen, Z.W. Yuan, and H.Y. Lu, Severe Plastic Deformation Techniques for Bulk Ultrafine-Grained Materials, *Rare Metal Mater. Eng.*, 2012, **41**(6), p 941–946
9. V. Yamakov, D. Wolf, S.R. Phillpot, A.K. Mukherjee, and H. Gleiter, Dislocation Processes in the Deformation of Nanocrystalline Aluminium by Molecular-Dynamics Simulation, *Nat. Mater.*, 2002, **1**(1), p 45–49
10. V. Yamakov, D. Wolf, S.R. Phillpot, and H. Gleiter, Dislocation–Dislocation and Dislocation–Twin Reactions in Nanocrystalline Al by Molecular Dynamics Simulation, *Acta Mater.*, 2003, **51**(14), p 4135–4147
11. Y.T. Zhu, X.L. Wu, X.Z. Liao, J. Narayan, L.J. Kecskes, and S.N. Mathaudhu, Dislocation–Twin interactions in Nanocrystalline fcc Metals, *Acta Mater.*, 2011, **59**(2), p 812–821
12. M.Y. Gutkin, I.A. Ovidkol, and N.V. Skiba, Crossover from Grain Boundary Sliding to Rotational Deformation in Nanocrystalline Materials, *Acta Mater.*, 2003, **51**(14), p 4059–4071
13. A.A. Fedorov, M.Y. Gutkin, and I.A. Ovidko, Transformations of Grain Boundary Dislocation Pile-Ups in Nano- and Polycrystalline Materials, *Acta Mater.*, 2003, **51**(4), p 887–898
14. C.P. Wang, F.G. Li, Q.H. Li, J. Li, L. Wang, and J.Z. Dong, A Novel Severe Plastic Deformation Method for Fabricating Ultrafine Grained Pure Copper, *Mater Des.*, 2013, **43**, p 492–498
15. C.P. Wang, F.G. Li, Q.H. Li, and L. Wang, Numerical and Experimental Studies of Pure Copper Processed by a New Severe Plastic Deformation Method, *Mater. Sci. Eng. A*, 2012, **548**(3), p 19–26
16. J.H. Li, F.G. Li, X.K. Ma, H. Chen, Z.C. Ma, and J. Li, Microhardness Distribution and Microstructural Evolution in Pure Aluminum Subjected to Severe Plastic Deformation: Elliptical Cross-Sectioned Spiral Equal-Channel Extrusion (ECSEE), *J. Mater. Eng. Perform.*, 2015, **24**(11), p 4543–4550
17. M.I. Latypov and K.H. Seop, Comparative Analysis of Two Twist-Based SPD Processes: Elliptical Cross-Section Spiral Equal-Channel Extrusion vs Twist Extrusion, *Mater. Trans.*, 2013, **54**(9), p 1587–1591
18. C.P. Wang, F.G. Li, H.Y. Lu, Z.W. Yuan, B. Chen, and H.J. Qiao, Deformation Analysis of Elliptical Cross-Section Spiral Equal Channel Extrusion Technique, *Rare Metal Mater. Eng.*, 2013, **42**(4), p 679–683
19. C.P. Wang, F.G. Li, and J.C. Liu, Deformational Features and Microstructure Evolution of Copper Fabricated by a Single Pass of the Elliptical Cross-Section Spiral Equal-Channel Extrusion (ECSEE) Process, *J. Mater. Eng. Perform.*, 2018, **27**(6), p 2967–2977
20. J.H. Li, F.G. Li, C. Zhao, H. Chen, X.K. Ma, and J. Li, Experimental Study on Pure Copper Subjected to Different Severe Plastic Deformation Modes, *Mater. Sci. Eng. A*, 2016, **656**, p 142–150
21. C.P. Wang, F.G. Li, H.Y. Lu, Z.W. Yuan, and B. Chen, Optimization of Structural Parameters for Elliptical Cross-Section Spiral Equal-Channel Extrusion Dies Based on Grey Theory, *Chin. J. Aeronaut.*, 2013, **26**(1), p 209–216

22. T. Hu, K. Ma, T.D. Topping, J.M. Schoenung, and E.J. Lavernia, Precipitation Phenomena in an Ultrafine-Grained Al Alloy, *Acta Mater.*, 2013, **61**(6), p 2163–2178

23. Y. Miyajima, S. Okubo, H. Abe, H. Okumura, T. Fujii, S. Onaka, and K. Masaharu, Dislocation Density of Pure Copper Processed by Accumulative Roll Bonding and Equal-Channel Angular Pressing, *Mater. Charact.*, 2015, **104**, p 101–106

24. R.Z. Valiev, R.K. Islamgaliev, and I.V. Alexandrov, Bulk Nanostructured Materials from Severe Plastic Deformation, *Prog. Mater Sci.*, 2000, **45**(2), p 103–189

25. A.S. Malin and M. Hatherly, Microstructure of Cold-Rolled Copper, *Mater. Sci.*, 1979, **13**(8), p 463–472

26. E. Bonnot, A.L. Helbert, F. Brisset, and T. Baudin, Microstructure and Texture Evolution During the Ultra Grain Refinement of the Armco Iron Deformed by Accumulative Roll Bonding (ARB), *Mater. Sci. Eng. A*, 2013, **561**(3), p 60–66

27. F. Salimyanfard, M.R. Toroghinejad, F. Ashrafizadeh, and M. Jafari, EBSD Analysis of Nano-Structured Copper Processed by ECAP, *Mater. Sci. Eng. A*, 2011, **528**(16–17), p 5348–5355

28. X. Molodova, G. Gottstein, M. Winning, and R.J. Hellmig, Thermal Stability of ECAP Processed Pure Copper, *Mater. Sci. Eng. A*, 2007, **s460-461**(1), p 204–213

29. A. Mishra, B.K. Kad, F. Gregori, and M.A. Meyers, Microstructural Evolution in Copper Subjected to Severe Plastic Deformation: Experiments and Analysis, *Acta Mater.*, 2007, **55**(1), p 13–28

30. S. Ferrasse, K.T. Hartwig, R.E. Goforth, and V.M. Segal, Microstructure and Properties of Copper and Aluminum Alloy 3003 Heavily Worked by Equal Channel Angular Extrusion, *Metall. Mater. Trans.*, 1997, **28**(4), p 1047–1057

31. J.Y. Huang, Y.T. Zhu, H. Jiang, and T.C. Lowe, Microstructures and Dislocation Configurations in Nanostructured Cu Processed by Repetitive Corrugation and Straightening, *Acta Mater.*, 2001, **49**(9), p 1497–1505

32. N. Hansen and R.F. Mehl, New Discoveries in Deformed Metals, *Metall. Mater. Trans. A*, 2001, **32**(12), p 2917–2935

33. N. Hansen and D.J. Jensen, Development of Microstructure in FCC Metals During Cold Work, *Philos. Trans. R. Soc. A Math. Phys. Eng. Sci.*, 1999, **357**(1756), p 1447–1469

34. Y. Wang, Y. Xin, H. Yu, L. Lv, and Q. Liu, Formation and Microstructure of Shear Bands During Hot Rolling of a Mg-6Zn-0.5Zr Alloy Plate with a Basal Texture, *J. Alloys Compd.*, 2015, **644**, p 147–154

35. V.M. Segal, Severe Plastic Deformation: Simple Shear Versus Pure Shear, *Mater. Sci. Eng. A*, 2002, **338**(1–2), p 331–344

36. A. Mishra, B.K. Kad, F. Gregori, and M.A. Meyers, Microstructural Evolution in Copper Subjected to Severe Plastic Deformation: Experiments and Analysis, *Acta Mater.*, 2007, **55**(1), p 13–28

37. N. Lugo, N. Llorca, J.M. Cabrera, and Z. Horita, Microstructures and Mechanical Properties of Pure Copper Deformed Severely by Equal-Channel Angular Pressing and High Pressure Torsion, *Mater. Sci. Eng. A*, 2008, **477**(1), p 366–371

38. Q. Liu, X. Huang, D.J. Lloyd, and N. Hansen, Microstructure and Strength of Commercial Purity Aluminium (AA 1200) Cold-Rolled to Large Strains, *Acta Mater.*, 2002, **50**(15), p 3789–3802

39. E. Nes, T. Pettersen, and K. Marthinsen, On the Mechanisms of Work Hardening and Flow-Stress Saturation, *Scr. Mater.*, 2000, **43**(1), p 55–62

40. M.J. Starink, X.G. Qiao, J. Zhang, and N. Gao, Predicting Grain Refinement by Cold Severe Plastic Deformation in Alloys Using Volume Averaged Dislocation Generation, *Acta Mater.*, 2009, **57**(19), p 5796–5811